1999

Skeletal Architecture and Density Banding Analysis Technique for Diploria strigosa by X-ray Computed Tomography

Kevin P. Helmle
Nova Southeastern University, kevinh@nova.edu

Richard E. Dodge (editor)
Nova Southeastern University, dodge@nova.edu

Proceedings 9th International Coral Reef Symposium, Bali, Indonesia 23-27 October 2000, Vol. 1, pp 365-371.

Skeletal architecture and density banding in *Diploria strigosa* by X-ray computed tomography

K. P. Helmle[1], R. E. Dodge[1], and R. A. Ketcham[2]

Abstract Density bands in corals have long been considered a valuable tool for reconstructing past environmental and climatic conditions. X-radiographs reveal density banding within a skeletal slab, but provide little information about the skeletal variability causing banding. The skeletal architecture of *Diploria strigosa* was analyzed by X-radiography, X-ray computed tomography, and image analysis to identify the specific skeletal elements responsible for density banding. Three-dimensional skeletal reconstructions, density-band reconstructions, and skeletal animations were created to assess the apparent changes in skeletal structure associated with density banding. Measurements were made of the dissepiments, thecae, septa, and columellae to determine how element size related to density banding. Dissepiment spacing and thecal wall thickness exhibited no consistent variation relative to density. Density bands were associated with thickening of septal and columellar structures. X-ray computed tomography provided an effective tool for revealing density banding as well as measuring variations in skeletal elements.

Keywords Coral skeleton, Density banding, Skeletal architecture, X-ray computed tomography

Introduction

Cyclic variations in skeletal structure of long-lived reef corals produce annual density bands evident by X-radiography and X-ray computed tomography. Corals generally accrete one high- and low-density skeletal band annually (Knutson *et al*. 1972, Dodge and Thompson 1974, Hudson *et al.* 1976, Wellington and Glynn 1983). Massive reef-building corals grow on the order of 1 $cm \cdot yr^{-1}$ over a life span of several centuries; because of this, density bands record growth over a long sequence of time. Density bands result from variations in coral growth, which reflect changing environmental conditions. The chronological reliability of density bands along with the chemical composition of the calcium carbonate ($CaCO_3$) skeleton provide valuable records for reconstructing past environmental and climatic conditions (Lough and Barnes 1990, Swart et al. 1996, Druffel 1997, Grottoli 1999).

Skeletal density has previously been shown to correlate with light (Knutson *et al.* 1972, Buddemeier 1974, Wellington and Glynn 1983,), temperature (Hudson *et al*. 1976, Highsmith 1979, Lough *et al.* 1999), cloud cover, and rainfall (Lough and Barnes 1990) on annual and seasonal timeframes. Skeletal records also reflect growth responses to anthropogenic perturbations such as sedimentation (Loya 1976, Dodge and Brass 1984, Barnes and Lough 1999), oil dispersants (Lewis 1971, Knap *et al.* 1983), and lead pollution (Dodge and Gilbert 1984). Because many factors can affect coral growth, it has proven difficult to define the environmental cause and physiological effect responsible for density-band formation. Identifying the skeletal basis of density banding is a necessary step and essential to accurately interpret banding patterns and the associated trace element and isotopic records (Dodge *et al.* 1992, Barnes and Lough 1996).

Due to variability across coral taxa and a lack of inter-species comparisons, the skeletal variations responsible for density banding are not completely understood. Buddemeier (1974) demonstrated that neither organic content nor trace element levels were substantial enough to cause the density variations associated with banding. Buddemeier *et al.* (1974) proposed two major alternatives for density-band formation: 1) the orderliness in which aragonite needles are deposited, and 2) the variation in size and spacing of the skeletal elements.

Barnes and Devereux (1988) termed the organization of aragonite needles or crystals as “micro-architecture” and the organization of skeletal elements (e.g., dissepiments, septa, and thecae) as “meso-architecture”. They analyzed the density of coral skeleton (*Porites*) by gamma-densitometry, buoyant weight, and powdered skeleton techniques and found that variations in micro-architecture were insufficient to account for density banding, further proposing a general thickening of the skeletal meso-architecture as the primary cause of density banding.

Dodge *et al.* (1992) analyzed the skeletal basis of density banding by image analysis of macro-photographs and X-radiographs of several *Montastraea annularis* colonies from South Florida, the Florida Keys, St. Croix, the Bahamas, and Mexico. Results were consistent at all sites and indicated that dissepiments and septa of the endotheca exhibited no systematic variation in thickness or spacing. They attributed high-density bands to increased thickening of exothecal dissepiments and costae.

The common trait of density-band formation, revealed by the work of Macintyre and Smith (1974), Emiliani *et al.* (1978), Barnes and Devereux (1988), Dodge *et al.* (1992), Barnes and Lough (1993), Taylor *et al*. (1993), Le

[1] K. P. Helmle and R. E. Dodge: Nova Southeastern University, Oceanographic Ctr. 8000 N. Ocean Drive, Dania Beach, FL, 33004 USA kevinh@nova.edu

[2] R. A. Ketcham: Department of Geological Sciences, C1110, University of Texas, Austin, TX, 78712 USA

Tissier *et al.* (1994), and others, is a thickening of meso-architectural skeletal elements associated with high-density bands.

Skeletal density has almost exclusively been measured by optical densitometry of X-radiographs and gamma densitometry of medially sectioned skeletal slabs (Buddemeier *et al.* 1974, Dodge and Brass 1984, Chalker *et al.* 1985, Chalker and Barnes 1990, Dodge *et al.* 2000). X-radiographs provide a picture of density variation that is subject to confounding variables associated with the orientation and overlap of skeletal structures (Barnes and Lough 1989, Barnes and Lough 1990, Barnes and Taylor 1993).

Le Tissier *et al.* (1994) found that X-radiograph apparent banding patterns are not solely the product of variations in skeletal thickening; rather, they can result from overlap of non-thickened skeletal structures based on their size and orientation to the X-ray beam. Further, they suggested that systematic variation in thickness of skeletal elements themselves, as opposed to banding patterns, provide the most accurate record of changes in coral growth.

High-resolution X-ray computed tomography (CT) provides images of coral skeleton which can be used to measure variations in thickness and spacing of skeletal elements while still providing a density-band pattern similar to that of an X-radiograph. Computed tomography has been used to assess coral bioerosion and bore holes (Hassan *et al.* 1994, Becker and Reaka-Kudla 1996), growth forms (Vago *et al.* 1994), growth bands (Logan and Anderson 1991), density, and calcification (Bosscher 1993, Heiss 1995).

Diploria strigosa (Dana 1848) is a common reef-building coral and a potentially important environmental recorder because it forms massive colonies, is abundant on western Atlantic and Caribbean reefs, and produces distinct annual density bands. *Diploria strigosa* has a meandroid (brain coral) growth form where linear series of polyps are separated by a skeletal wall called a theca (Fig. 1). Adjacent rows of polyps share a common theca; therefore, no exothecal structures are present. The thinner vertical inner walls are called septa. Opposing rows of septa anastamose, or join, to form a spongy structure called the columella. As the colony grows, polyps lift their basal surface and secrete new floors, or dissepiments. Tabular dissepiments are relatively flat structures; whereas, vesicular dissepiments are typically shorter connective structures between the more continuous tabular dissepiments (for further discussion of terms and structures, see Wells 1956).

In this paper we report on the relationships between skeletal architecture and density banding in *Diploria strigosa.* This relationship was examined using high-resolution X-ray computed tomography and computer-image analysis. We focused on the skeletal meso-architecture and considered the size and shape of dissepiments, thecae, septa, and columellae associated with high-density (HD) and low density (LD) bands.

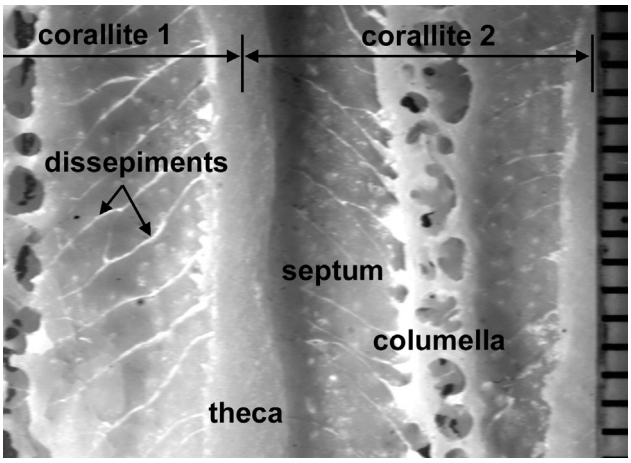

Fig. 1 Longitudinal section of *Diploria strigosa* showing the skeletal structures: dissepiments, theca, septum, and columella. The image illustrates the thinness of the tabular and vesicular dissepiments, the irregular columella, and the lack exothecal structures between adjacent corallites. Each bar of the scale represents 0.5 mm intervals

Methods

Four specimens of the scleractinian coral, *Diploria strigosa*, were collected on December 12, 1985, at a 6 m depth off Hollywood Beach, Florida. X-radiographs of the specimens revealed distinct, regular density bands. Dodge *et al.* (1992) showed conspecific corals from different locations exhibited consistent skeletal variations relative to density banding; therefore, a single coral specimen was selected for skeletal analysis. The colony measured 35 cm in diameter and 15 cm in height. The coral was sectioned medially producing two parallel-sided slabs 6-7 mm thick. Slabs were X-radiographed with a setting of 50 kvP and 10 ma for 9 seconds and contained a growth record of 31 yrs (1955-1985). The uppermost sections of the slabs, representing the top of the colony, were sectioned into eight approximately equal sized pieces (50x70 mm). Seven pieces were ground on a geologists thin-section maker at 0.25-mm intervals. Images were captured at each 0.25-mm interval with a flatbed scanner. The eighth piece was further sectioned parallel to and through the middle of ten high-density (HD) and ten low-density (LD) bands based on their location from the X-radiograph. The 20 plan-view skeletal surfaces from the HD and LD bands were imaged using a flatbed scanner.

For CT analysis, a coral cube measuring 25 mm on a side was sectioned so the top of the cube was a plan-view of the skeleton and the sides ran parallel to the growth axis. The cube was scanned at the High-Resolution X-ray CT Facility at the University of Texas at Austin, described by Ketcham and Carlson (2001). Settings for the scans were 100 kV and 0.325 mA, resulting in a focal spot of approximately 0.035 mm. Acquisition times of 90 seconds were used to construct 512x512 pixel images. The cube was positioned so that the plane of X-rays ran perpendicular to the growth axis producing plan-view images and 42 consecutive 0.1-mm-thick slices were scanned at 0.2-mm intervals, representing 8.4 mm of skeleton (Fig. 2a). The cube was then oriented so the plane of X-rays ran parallel to the growth axis producing longitudinal-view image and 30 consecutive 0.1-mm-thick slices were scanned at 0.1-mm intervals, representing 3.0 mm of skeleton (Fig. 2b). Fortner Slicer 3-D software (Fortner Res. LLC, Sterling VA 20164) was used to render these three-dimensional skeletal reconstructions from the CT images. With a reduced image opacity, the 3-D

skeletal reconstructions were rotated and tilted to assess the orientation of density bands to the slab. This was a useful technique for determining whether the bands were the product of variations in skeletal thickness or rather the byproduct of fortuitously aligned structures within the slab.

The 30 longitudinal-view images (e.g., Fig. 3a) were used to reconstruct the density-band pattern. The opacity of each image was reduced and the images were overlaid to form a single image or two-dimensional reconstruction (Fig. 3b). Consecutive CT images were also linked as AVI files to produce animations traveling through the coral skeleton. Longitudinal-view images were linked to create an animation passing through the skeleton parallel to the density bands. Plan-view images were linked to create an animation passing through the skeleton perpendicular to the density bands (Fig. 4). The plan-view animation included a picture in picture (PIP) window with a longitudinal-view slab that showed the density bands. The PIP window included a reference line that moved along the longitudinal-view slab indicating the location of the plan-view animation within HD and LD bands.

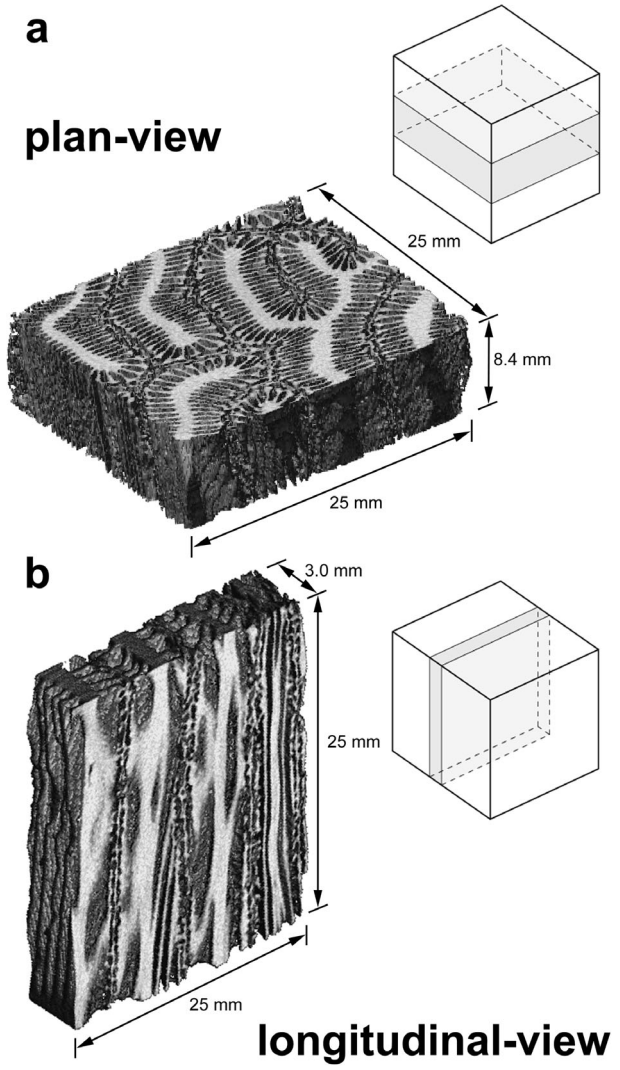

Fig. 2 Three-dimensional skeletal reconstructions of X-ray CT images and their relative positions within a diagram of the 25x25x25 mm coral cube: (a) 42 plan-view images and (b) 30 longitudinal-view images. Coral cube diagrams are oriented with the growth trajectory running vertically.

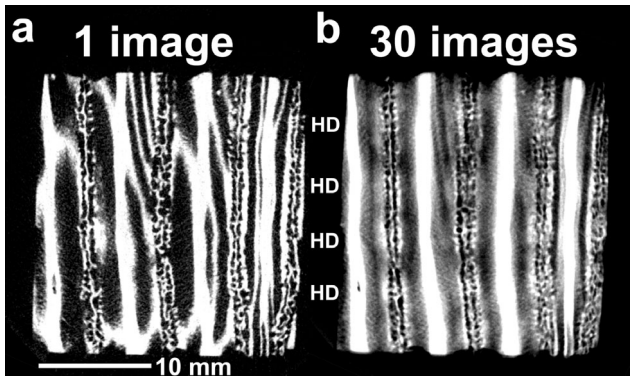

Fig. 3 (a) Longitudinal-view X-ray CT image represents a 0.1-mm-thick skeletal slab. (b) Two-dimensional density-band reconstruction compiled from 30 consecutive images represents a 3.0-mm-thick skeletal slab. Light bands represent high density (HD) skeleton on the 2-D reconstruction.

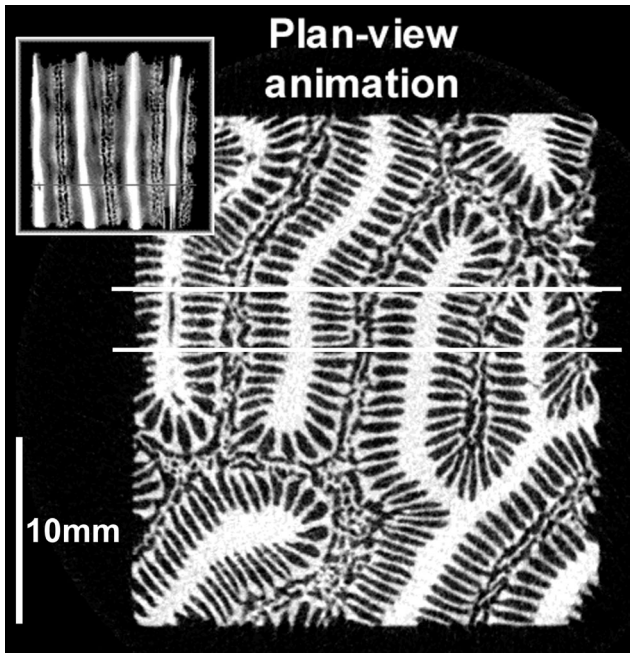

Fig. 4 Still-frame of plan-view animation with inset of longitudinal view slab (upper left). White lines on the plan view indicate the thickness and location of the longitudinal-view slab. Grey line on the inset slab indicates the location of the plan-view animation within high- and low-density bands. (http://www.nova.edu/ocean/khelmle/diploriamovie.html)

Measurements were made of dissepiment spacing and thecal wall thickness on computer images of the sectioned skeletal slabs. Measurements were made by computer image analysis (Mocha software, Jandell Scientific, San Rafael CA 94901).

Using images from thin-sectioned slabs, dissepiment spacing was measured along 13 transects taken mid-way between the theca and columella. Transects were 10-30 mm long, included 13-36 dissepiments, and spanned at least two HD and two LD bands. Density-band boundaries were determined from optic density measurements on the X-radiographs. A dissepiment spacing measurement was also taken at the maximum and minimum density value of each band in order to isolate possible spacing variations. Dissepiment thickness was consistently less than 0.01 mm.

Thecal wall thickness was measured on images from ten HD and ten LD plan-view slabs. Thicknesses, or widths, across the thecal wall were measured in the same position on HD and LD slabs. From 36-43 thickness measurements per density band were collected. A total of 20 slabs representing ten growth years were analyzed.

Average pixel intensity (API) was measured on plan-view CT images by calculating the mean pixel grayscale value within rectangular regions of interest (ROIs) encompassing thecae, septa, and columellae (4.6 mm^2, 6.6 mm^2, and 4.6 mm^2, respectively). The ROIs were located over constant skeletal positions from image to image. Pixel grayscale values corresponded to the average X-ray attenuation within the volume of skeleton encompassed by the pixel boundaries and the scan thickness. Values ranged from 0 to 255, with low values signifying air, high values signifying skeletal material, and middling values representing a mixture of the two. There was some blurring across pixels caused by the finite resolution of CT data, which affected individual pixel values, but did not affect the overall amount of X-ray attenuation recorded in the image. By using averages within ROIs, the edge effects caused by blurring were eliminated, and changes in API could thus be directly interpreted as changes in skeletal element thickness. The principles of this technique were identical to those used for measuring porosity and fracture thickness in rocks using CT (see discussion and references in Ketcham and Carlson, 2001).

Data were analyzed with SAS/STAT software (SAS Institute Inc., Cary NC 27513). One-way ANOVA's were used for comparison of HD and LD data sets within individual transects. A General Linear Model (GLM) was employed where unbalanced data sets occurred. Two-way ANOVA's were used for comparisons of HD and LD data sets among transects.

Results

The longitudinal-view images (Fig. 3a) represented X-rays of 0.1-mm-thick coral slabs with the thecae, columellae, septa, and dissepiments apparent. No clear banding pattern was present in the 0.1-mm individual images. The two-dimensional reconstruction of density bands (Fig. 3b) created from the 30 consecutive longitudinal-view images exhibited a clear banding pattern.

The longitudinal-view animation was created from 30 X-ray CT images (0.1 mm thick, 0.1 mm intervals). This animation traveled through the coral parallel to the density bands over a distance of 3.0 mm and revealed no obvious trends in skeletal structure. The plan-view animation (Fig. 4), created from 42 X-ray CT images (0.1 mm thick, 0.2 mm intervals), allowed the viewer to travel through 8.4 mm of coral skeleton deposited over approximately two years i.e., 2 HD and 2 LD bands. The picture in picture display located the plan-view animation as it passed through HD and LD bands. Thickening of both septa and columellae were observed in HD skeleton; whereas, no change in thickness of the thecae was apparent (animation available via internet at http://www.nova.edu/ocean/khelmle/diploriamovie.html).

Mean dissepiment spacing did not differ significantly between HD and LD bands for any of the individual 13 transects (One-Way ANOVA, α=0.05, n=13-36). Nor did the overall mean dissepiment spacing, for all 13 transects combined, differ significantly between HD and LD bands (GLM Two-Way ANOVA, p=0.559, d.f. 1, 316). Dissepiment spacing measured at high- and low-density extremes (i.e., HD maxima and LD minima) was significantly smaller at maxima HD values (GLM Two-Way ANOVA, p=0.017, d.f. 1, 121).

Mean thecal wall thickness was not significantly different between HD and LD bands in eight of ten years (One-Way ANOVA, α=0.05, n=36-43). For the other two years, thickness was greater in the HD band of one (p=0.003, n=43) and greater in the LD band of the other (p<0.001, n=43). No significant difference existed in mean thecal wall thickness between HD and LD bands for the ten years combined (GLM Two-Way ANOVA, p=0.673, d.f. 1, 810), a significant level of interaction was present between HD/LD comparison and year by year comparison.

Thecal, septal, and columellar thickness was assessed as a function of average pixel intensity (API) on X-ray CT images. Consistent with annual thecal wall thickness measurements, the API of thecal regions did not differ significantly between HD and LD bands (Fig. 5)(Two-Way ANOVA, p=0.126, d.f. 1, 39). In contrast the API was significantly greater within HD bands for septal regions (Fig. 5)(Two-Way ANOVA, p=0.003, d.f. 1, 39) and columellar regions (p<0.001, d.f. 1, 39).

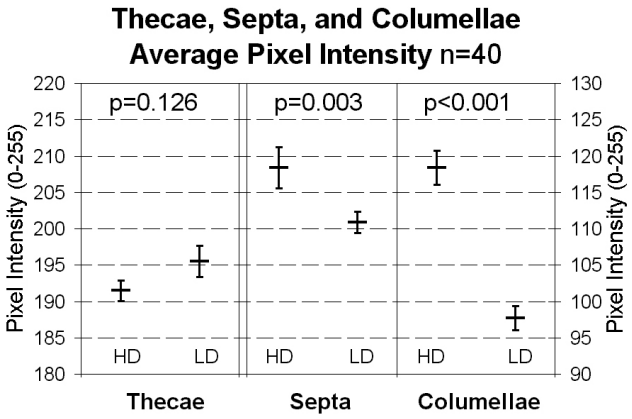

Fig. 5 Average Pixel Intensity (API) of thecae, septa, and columellae for high-density (HD) and low-density (LD) bands. An increase in API values indicates the presence of more skeleton. Error bars represent ± 1 standard error. Significance levels based on a two-way ANOVA for HD and LD bands and regions within bands.

Discussion

The individual 0.1-mm-thick longitudinal-view X-ray CT images had no apparent banding pattern (Fig. 3a). The lack of apparent banding does not indicate a lack of variability in skeletal element thickness; rather, it indicates that the amount of skeletal variation added up over a 0.1-mm-thick skeletal slice was insufficient to produce apparent density bands. The two-dimensional density-band reconstruction, created from 30 consecutive 0.1-mm-thick images, had distinct bands resulting from skeletal element thickness variations aligned over 3.0 mm of reconstructed skeleton (Fig. 3b). The reconstructed

banding pattern supports the finding of Barnes and Devereux (1988), Dodge *et al.* (1992), Le Tissier *et al.* (1994) and others, that X-ray revealed density banding is the product of skeletal element thickness variations.

The presence of banding at 3.0 mm and absence at 0.1 mm of skeleton indicates that apparent banding patterns are not consistently representative of variations in element thickness. Le Tissier *et al.* (1994) showed that structures as thin as 10 μm can cause fine banding depending on the orientation and path length of the structure. While unnoticeable in the 0.1-mm-thick slices, such fine bands may have been present; however, the reconstructed banding pattern appeared to result primarily from aligned variations of the septa, and columellae.

The plan-view animation (Fig. 4) passed through more than two years of skeleton and showed periodic trends in element thickness as the animation passed through consecutive HD and LD bands. The plan-view animation exhibited obvious thickening of septa and columellae associated with HD bands. No apparent changes in the thecae were evident. The plan-view animation clearly illustrated that skeletal variations in meso-architecture were associated with the location of HD and LD bands.

The longitudinal view animation passed through the skeleton normal to the growth axis. No apparent trends in element thickness were observed. This does not indicate a lack of skeletal variation, rather it suggests that the majority of thickening, responsible for banding, primarily occurs normal to the growth axis in *Diploria strigosa*.

Diploria strigosa deposits an average of six tabular dissepiments per year (n=50) that are on the order of 0.01 mm thick. Dissepiment spacing was not found to be significantly different between HD and LD bands, except at the HD maxima and LD minima. Le Tissier *et al.* (1994) calculated that dissepiments less than 0.02 mm thick will not be expressed on X-radiographs unless oriented at an angle to the X-ray beam. Considering the spacing measurements and the extreme thinness of dissepiments, it seems unlikely that dissepiments substantially contribute to bulk-density variations responsible for banding in *D. strigosa*.

The average thickness of the thecal wall was about 1.6 mm. Thecal wall thickness was measured on plan-view slabs from ten HD and ten LD bands. Mean HD thickness, for all ten years combined, was not significantly different from mean LD thickness. There was a significant level of interaction because changes in meandroid growth of the colony over the ten-year period were greater than thickness variations between HD and LD bands. To account for this, thickness was compared only between HD and LD bands of the same year. Eight of the ten years exhibited no significant difference in thickness between HD and LD bands. Thecal wall thickness measured by API did not differ significantly between HD and LD bands. The thecal API results are less robust than septal and columellar results at indicating skeletal thickening due to the large skeleton-to-air-space ratio. Considering that the thecal API results supported the actual skeletal thickness measurements, no consistent thickening of the thecae was associated with density-band formation.

In *Diploria strigosa*, septa possess paliform lobes (vertical pillar-like structures at inner edges of septa), synapticulae (small horizontal rods connecting adjacent septa), and septal teeth (tiny spikes and protrusions on the septa). Because API measurements represented the amount of skeleton present in a given area on the image, they encompassed possible variations in these secondary structures. Septal thickness was significantly greater in HD bands. The significant increase in API reflected thickening of the septa because the location, the number of septa, and the CT settings were all held constant. API measurements were useful because thickness was not consistent along the length of a septum; they were thinnest near the middle and thickened approaching the theca and at their inner margins.

The columella of *Diploria strigosa* is formed by anastamosing along the inner margins of the septa forming a loosely organized structure. Columellar API was significantly greater in HD bands. *Diploria strigosa* possesses a highly irregular trabecular columella; therefore, the significantly greater API signified thickened and/or increased columellar structure. API measurements were ideal for measuring the complex septal and columellar structure, which were not conducive to simple point-to-point thickness measurements. The results confirmed the apparent variations in septal thickness and columellar structure visible in the plan-view animation.

It is evident in the literature that the specific skeletal elements causing density banding differ between species (Macintyre and Smith 1974, Barnes and Devereux 1988, Dodge *et al*. 1992, Le Tissier *et al*. 1994, and others). This study of *Diploria strigosa* is the first analysis of density banding for a meandroid coral. Our general results indicated that apparent density bands in *D. strigosa* resulted from thickness variations in the septa and columellae. The location of density bands within skeletal slabs supported these findings as banding was typically limited to sections of septa and columellae.

A distinction exists between skeletal element thickness variations and the resultant banding pattern produced on X-radiographs. Thickness or spacing variations in skeletal elements generally result from changes in the extension rate and/or calcification rate of the coral in response to varying environmental conditions or endogenous processes. Density bands on X-radiographs typically provide little information about the actual skeletal variations that cause them. Barnes and Lough (1990), Barnes and Taylor (1993), and Le Tissier *et al.* (1994) extensively illustrated the effects of skeletal architecture on X-ray apparent density bands and the possible misinterpretations. This paper identifies the variations in specific skeletal elements causing banding in *Diploria strigosa*. Further, the research illustrates techniques for linking the assessment of skeletal element variations with the resultant density-band pattern by X-ray computed tomography.

Acknowledgements We thank Dr. Dave Barnes and an anonymous reviewer for their comments and suggestions. We thank Kevin Kohler for computer support on this project.

References

Barnes DJ, Devereux MJ (1988) Variations in skeletal architecture associated with density banding in the hard coral *Porites*. J Exp Mar Biol Ecol 121:37-54

Barnes DJ, Lough JM (1989) The nature of skeletal density banding in scleractinian corals: fine banding and seasonal patterns. J Exp Mar Biol Ecol 126:119-134

Barnes, DJ, Lough JM (1990) Computer simulations showing the likely effects of calix architecture and other factors on retrieval of density information from coral skeletons. J Exp Mar Biol Ecol 137:141-164

Barnes DJ, Lough JM (1993) On the nature and cause of density banding in massive coral skeletons. J Exp Mar Biol Ecol 167:91-108

Barnes DJ, Taylor RB (1993) On corallites apparent in X-radiographs of skeletal slices of *Porites*. J Exp Mar Biol Ecol 173:123-131

Barnes DJ, Lough JM (1996) Coral skeletons: storage and recovery of environmental information. Global Change Biol 2:569-582

Barnes DJ, Lough JM (1999) *Porites* growth characteristics in a changed environment: Misima Island, Papua New Guinea. Coral Reefs 18:213-218

Becker LC, Reaka-Kudla ML (1996) The use of tomography in assessing bioerosion in corals. Proc 8th Int Coral Reef Symp 2:1819-1824

Bosscher H (1993) Computerized tomography and skeletal density of coral skeletons. Coral Reefs 12:97-103

Buddemeier RW (1974) Environmental controls over annual and lunar monthly cycles in hermatypic coral calcification. Proc 2nd Int Coral Reef Symp 2:259-267

Buddemeier RW, Maragos JE, Knutson DW (1974) Radiographic studies of reef coral exoskeletons: rates and patterns of coral growth. J Exp Mar Biol Ecol 14:179-200

Chalker B, Barnes D, Isdale P (1985) Calibration of X-ray densitometry for the measurement of coral skeletal density. Coral Reefs 4:95-100

Chalker B, Barnes DJ (1990) Gamma densitometry for the measurement of skeletal density. Coral Reefs 9:11-23

Dana JD (1848) Zoophytes. United States Exploring Expedition during the Years 1838-1842 under the Command of Charles Wilkes. vol 7, pp 121-708

Dodge RE, Thomson J (1974) The natural radiochemical and growth records in contemporary hermatypic corals from the Atlantic to the Caribbean. Earth Planet Sci 36:339-356

Dodge RE, Brass GW (1984) Skeletal extension, density, and calcification of the reef coral, *Montastrea annularis*: St. Croix, U.S. Virgin Islands. Bul Mar Sci 34:288-307

Dodge RE, Gilbert TR (1984) Chronology of lead pollution contained in banded coral skeletons. Mar Biol 82:9-13

Dodge RE, Szmant AM, Garcia R, Swart PK, Forester A, Leder JJ (1992) Skeletal structural basis of density banding in the reef coral *Montastraea annularis*. Proc 7th Int Coral Reef Symp 1:186-195

Dodge RE, Kohler KE, Helmle KP (2000) Coral skeletal densitometry analysis program: CORDAP. Presented poster: 9th Int Coral Reef Symp

Druffel ERM (1997) Geochemistry of corals: Proxies of past ocean chemistry, ocean circulation, and climate. Proc Natl Acad Sci 94:8354-8361

Emiliani C, Hudson JH, Shinn EA, George RY (1978) Oxygen and carbon isotopic growth in a reef coral from the Florida Keys and in a deep-sea coral from Blake Plateau. Science 202:627-629

Grottoli AG (1999) Variability of stable isotopes and maximum linear extension in reef-coral skeletons at Kaneohe Bay, Hawaii. Mar Biol 135:437-449

Hassan M, Dullo W, Fink A (1997) Assessment of boring activity in Porites lutea from Aqaba (Red Sea) using computed tomography. Proc 8th Int Coral Reef Symp 2:1813-1818

Heiss GA (1995) Carbonate production by scleractinian corals at Aqaba, Gulf of Aqaba, Red Sea. Facies 33:19-34

Highsmith RC (1979) Coral growth rates and environmental control of density banding. J Exp Mar Bio Ecol 37:105-125

Hudson JH, Shinn EA, Halley RB, Lidz B (1976) Sclerochronology: a tool for interpreting past environments. Geology 4:361-364

Ketcham RA, Carlson WD (2001) Acquisition, optimization and interpretation of X-ray computed tomographic imagery: Applications to the geosciences. Computers and Geosciences 27:381-400

Knap AH, Sleeter TD, Dodge RE, Weyers SC, Frith HR, Smith SR (1983) The effects of oil spills and dispersants use on corals: a review and multidisciplinary approach. Oil Pertochem Poll 1:157-169

Knuston DW, Buddemeier RW, Smith SV (1972) Coral chronometers: seasonal growth bands in reef corals. Science 177:270-272

Le Tissier MD'AA, Clayton B, Brown BE, Davis PS (1994) Skeletal correlates of coral density banding and an evaluation of radiography as used in sclerochronology. Mar Ecol Prog Ser 110:29-44

Lewis JB (1971) Effects of crude oil and oil spill dispersant on reef corals. Mar Pollut Bull 2:59-62

Logan A, Anderson IH (1991) Skeletal extension growth rate assessment in corals, using CT scan imagery. Bull Mar Sci 49:847-850

Lough JM, Barnes DJ (1990) Possible relationships between environmental variables and skeletal density in a coral colony from the Great Barrier Reef. J Exp Mar Biol Ecol 134:221-241

Lough JM, Barnes DJ, Devereux MJ, Tobin BJ, Tobin S (1999) Variability in growth characteristics of massive *Porites* on the Great Barrier Reef. CRC Tech Report No. 28

Loya Y (1976) Effects of water turbidity and sedimentation on the community structure of Puerto Rican corals. Bull Mar Sci 26:450-460

Macintyre IG, Smith SV (1974) X-radiographic studies of skeletal development in coral colonies. Proc 2nd Int Coral Reef Symp 2:277-287

Swart PK, Healy G, Dodge RE, Kramer P, Hudson H, Halley R, Robblee M (1996) The stable oxygen and carbon isotopic record from a coral growing in Florida Bay: a 160-year record of climatic and anthropogenic influences. Palaeo Palaeo Palaeo 123:219-237

Taylor RB, Barnes DJ, Lough JM (1993) Simple models of density band formation in massive corals. J Exp Mar Biol Ecol 167:109-125

Vago R, Shai Y, Ben-Zion M, Dubinsky Z, Achituv Y (1994) Computerized tomography and image analysis: A tool for examining the skeletal characteristics of reef-building organisms. Limnol Oceanogr 39,448-452

Wellington GM, Glynn PW (1983) Environmental influences on skeletal banding in the eastern Pacific (Panama) corals. Coral Reefs 1:215-222

Wells JW (1956) Scleractinia. In: Treatise on invertebrate paleontology, Part F, *Coelenterata*, Ed RC Moore, Geological Society of America, Univ of Kansas Press, Lawrence, KA. pp 328-403